Supplementary material: How ice apron loss and permafrost degradation promote the Platteikogel rock slide: A thermo-mechanical reconstruction

Felix Pfluger[1], Samuel Weber[2, 3], Natalie Barbosa[1,4], Florentin Hofmeister[5], Johannes Leinauer[1], Peter Wegmann[6], and Michael Krautblatter[1]

[1]Landslide Research Group, TUM School of Engineering and Design, Technical University of Munich, Munich, Germany
[2]WSL Institute for Snow and Avalanche Research, SLF, Davos Dorf, Switzerland
[3]Climate Change, Extremes and Natural Hazards in Alpine Regions Research Center CERC, Davos Dorf, Switzerland
[4]Department of Earth and Environmental Sciences, Faculty of Earth Sciences, GeoBio Center, Ludwig Maximilians University, Munich, Germany
[5]Bavarian Academy of Sciences and Humanities, Geodesy and Glaciology, Alfons-Goppel Str. 11, 80539 Munich, Germany.
[6]Department of Computer Science, TUM School of Computation, Information and Technology, Technical University of Munich, Munich, Germany

Correspondence: Felix Pfluger (felix.pfluger@tum.de)

This document contains Supplementary Material only, identified by the label "SM".

Contents

1 Supplementary Figures **2**

2 Supplementary Tables **8**

3 Discussion - Scope of interpretation and limitations to modeling **9**

3.1 Implications and limitations of the mechanical analysis with UDEC 9

3.2 Representation and limits of thermal processes in CryoGrid 2D 9

References **10**

1 Supplementary Figures

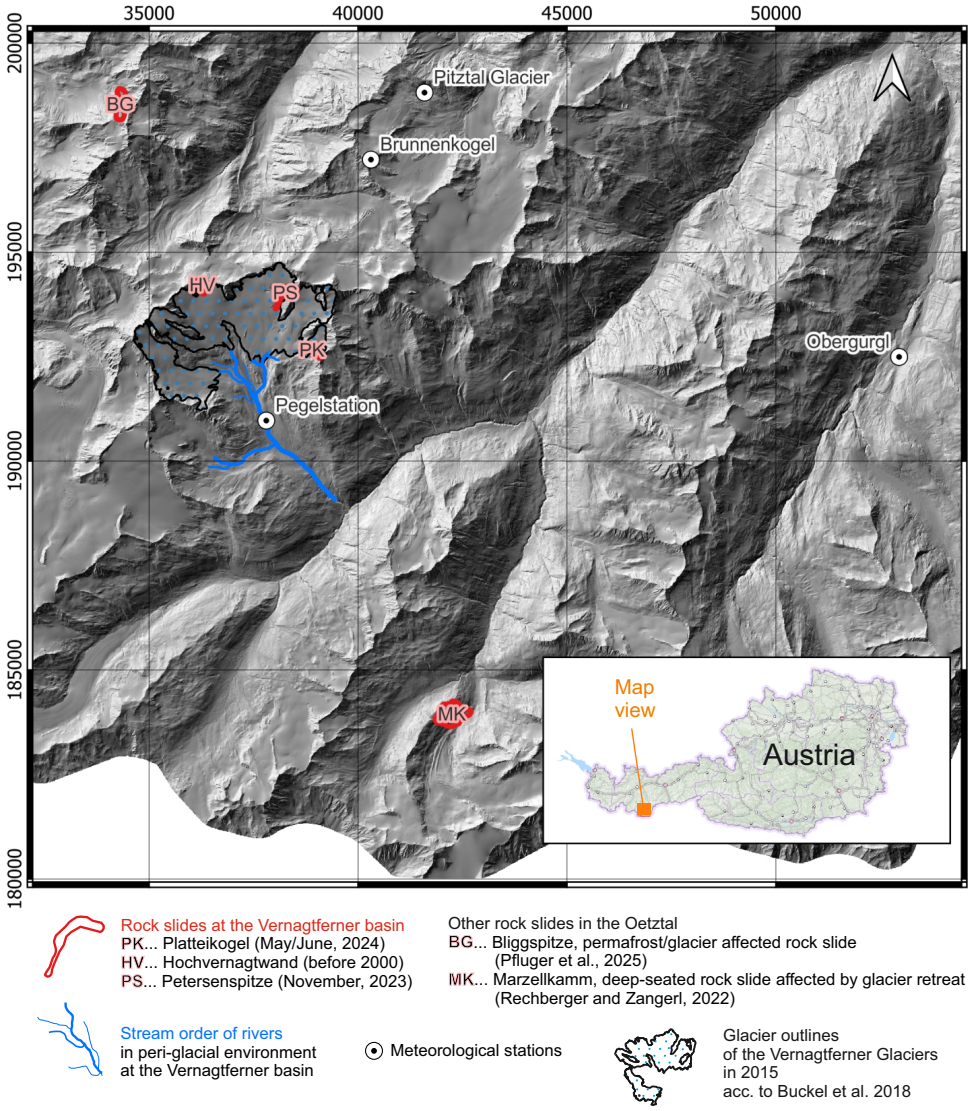

Figure SM1. Expanded overview including the study site at the Vernagt Basin in the Ötztal Alps, the position of the meteorological stations, of which data was used to model RST for the CryoGrid 2D simulations, prominent rock slides at Vernagtferner and rock slides studied in other scientific literature in neighboring valleys (Rechberger and Zangerl, 2022; Pfluger et al., 2025). The location of the hydrometeorological station "Pegelstation" of the Bavarian Academy of Sciences (BAdW) is shown at the glacier forefield. Data source: Basemap is DEM of 2017 provided by Land Tirol - https://www.tirol.gv.at/data/ (last access: 7 January 2025), glacier outlines of 2018 according to Buckel and Otto (2018) . Note: An interactive web map produced by the AlpSenseRely project highlights geomorphologic changes in valleys of Oetztal between 2015 and 2022, and clusters phenomena by rock- or ice-falls, slides, and sedimentological redistributions: https://og.realitymaps.de/AlpSenseRely/; last accessed, 20.02.2025.

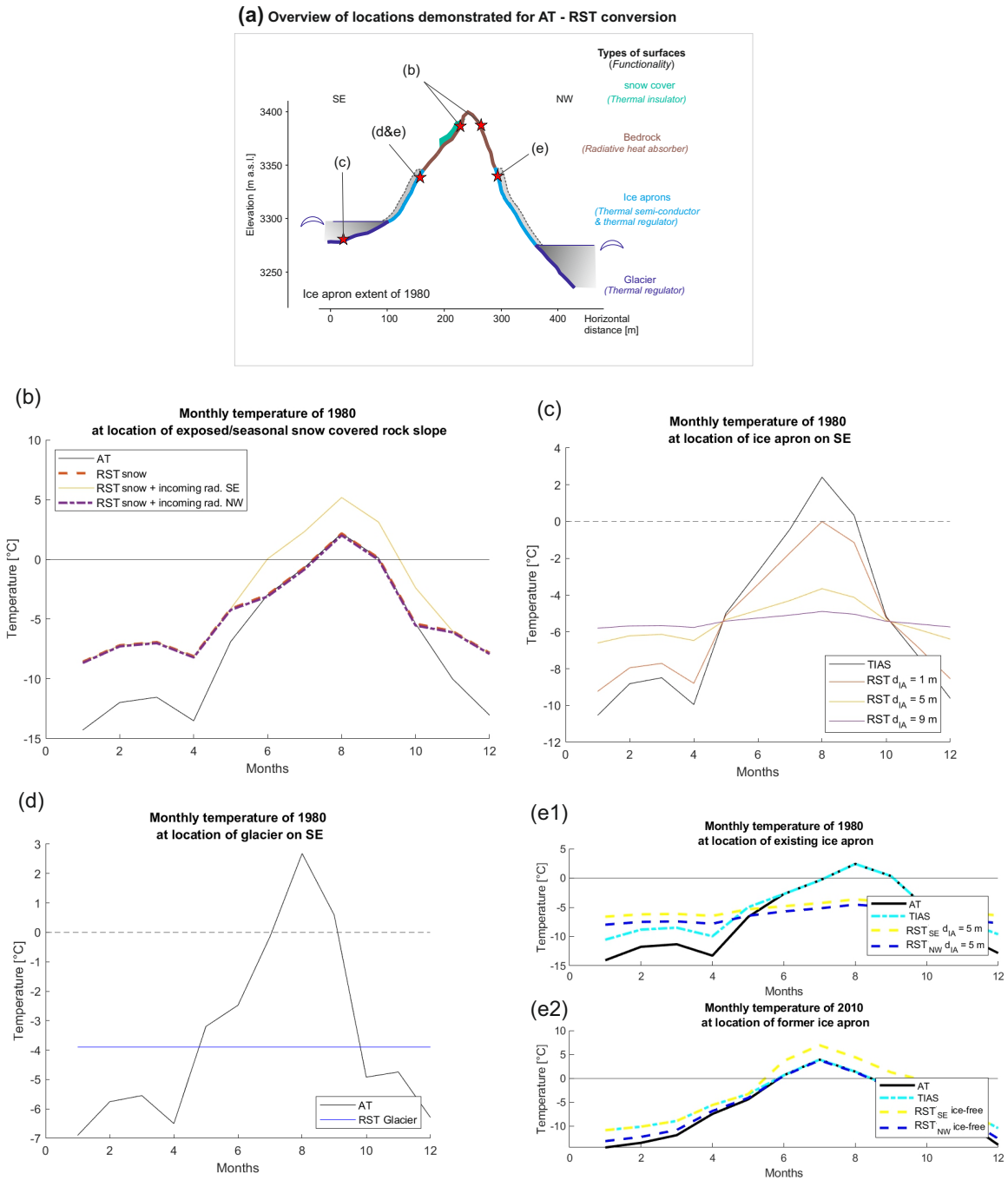

Figure SM2. Demonstration of AT-RST conversion for specified locations along topography (a) by using Eqs. 1 to 4 in order to consider different surface types (b-e). (b) Demonstration of the insulating effect of snow cover (Eq. 1), and radiative warming of sun-exposed bedrock (Eq. 2) using +3°/0°C surface offset for SE/NW aspects. (c) Seasonal amplitude inferred for the ice apron–bedrock boundary as a function of ice apron thickness (Eq. 3). (d) Glacier bed temperature is not influenced by seasonal amplitude (Eq. 4, nF-factor = 0.5). RST before (e1) and after (e2) ice apron loss, demonstrated for SE and NW aspect.

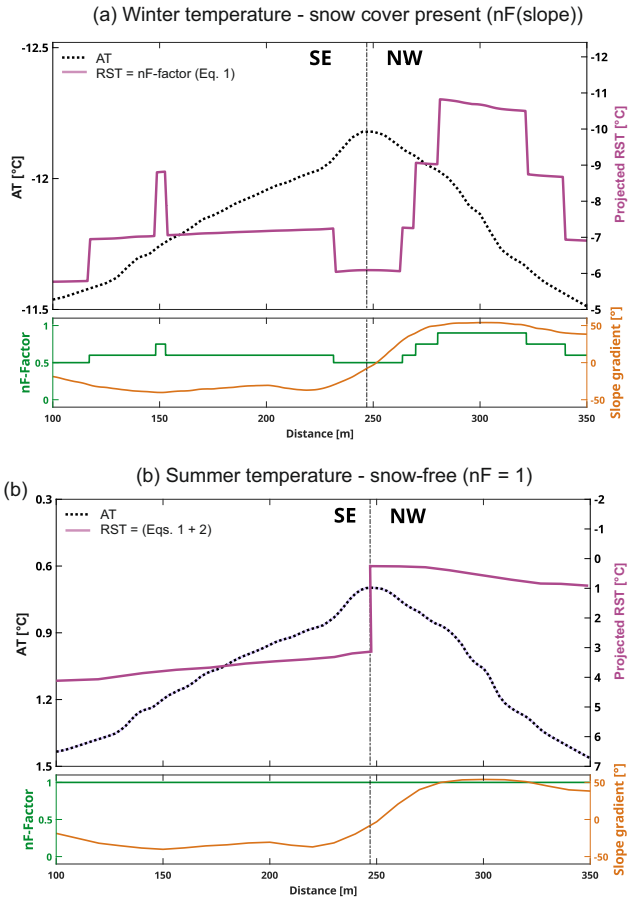

Figure SM3. Demonstration of AT-RST conversion along profile topography for a month with (a) snow cover (Eq. 1) and (b) without snow cover, but with radiative warming (Eq. 2) in the area of the Platteikogel peak. The y-axis is inverted to demonstrate the form of the AT resembling the mountain topography. Note: The lower plots indicate the deviation of the nF-scaling factor from the slope of the mountain; for snow-free months, nF is set to 1.

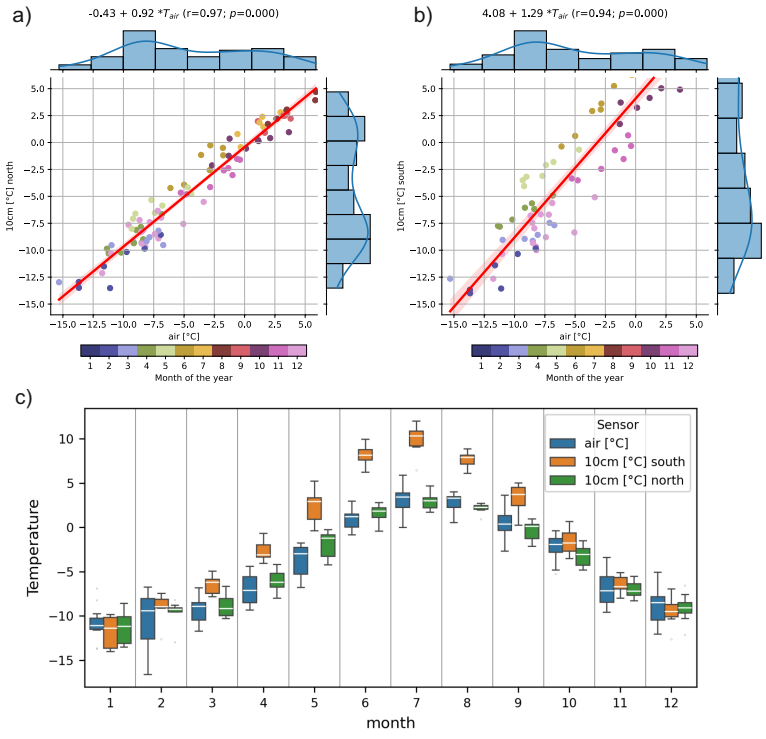

Figure SM4. Comparison of measured air temperature to rock temperature at 0.1m depth - as a common proxy for RST - for (a) north and (b) south facing rock wall at the Matterhorn Hörnli ridge at approx. 3500 m a.s.l. The data was aggregated to mean monthly values (Table A1, v). The linear regression models indicate the magnitude of the AT-RST offsets. (c) Boxplots demonstrate distinct differences between north- and south-exposed RST during the summer months. Note: Each individual boxplot contains between 6 and 8 data points.

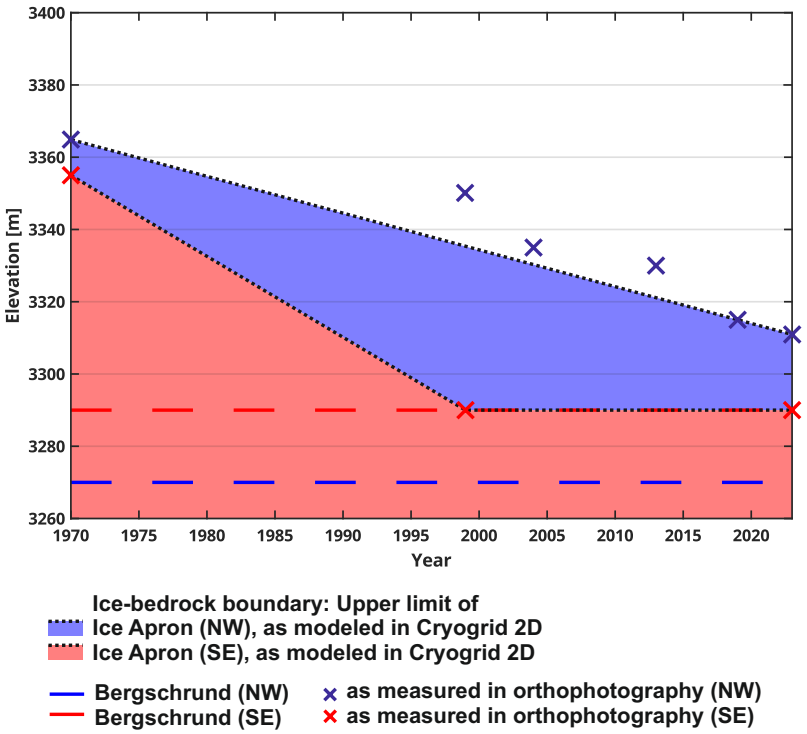

Figure SM5. Ice apron retreat and location of the Bergschrund as mapped from orthophotos. The derived linear model of ice apron retreat was implemented in the forcing of the Cryogrid 2D simulations. Note: The bergschrund was mapped at the same time as ice arpons; its position varied less than 5 m horizontally throughout observation time.

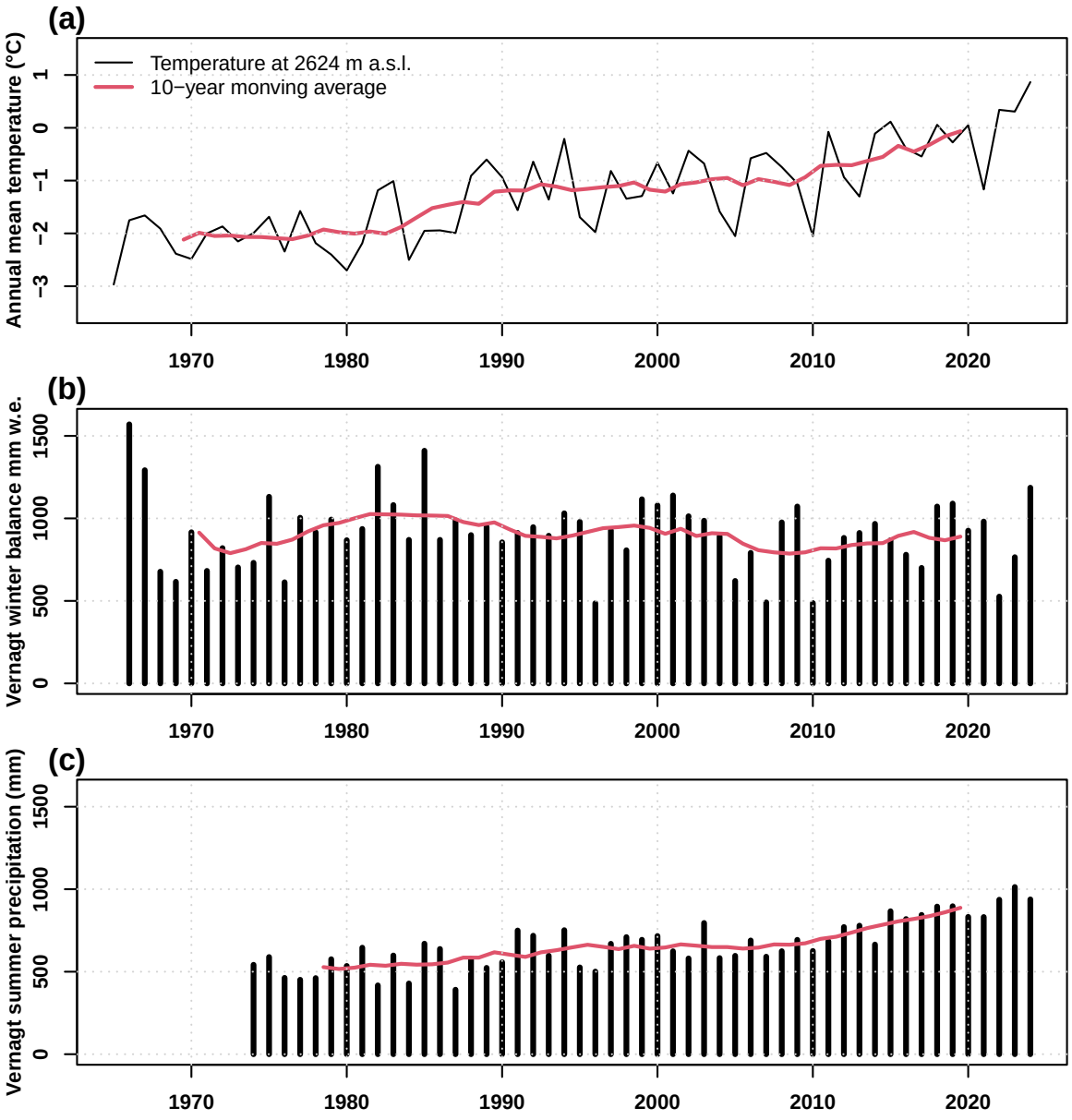

Figure SM6. Long-term meteorological observations of the Bavarian Academy of Sciences (BAdW) at the Vernagtferner (2624 m a.s.l., location see Fig.SM1) since 1964, including (a) air temperature (extrapolation based on the Obergurgl station), (b) winter mass balance (i.e., October to May) as proxy for solid precipitation, and (c) measured liquid precipitation (i.e., June to September). The red line shows the 10-year moving average. Note: The air annual temperature (a) was extrapolated from the Obergurgl station (1938 m a.s.l., Table A2, iii) to the Vernagtferner Pegelstation using a mean lapse rate of -0.496 °C/100m. This lapse rate was computed with temperature records of both stations covering the period from 1994 to 2023.

2 Supplementary Tables

Table SM1. General parameters utilized in all simulations with CryoGird 2D.

Mesh			
Equidistance of nodes along topography	0.05 m	acc. to Myhra et al. (2017, 2019); Czekirda et al. (2023)	
Depth z dependend resolution	Depth	Equidistance of nodes	acc. to Myhra et al. (2017, 2019); Czekirda et al. (2023)
	0 m - 2 m	1 m	
	2 m - 10 m	10 m	
	10 m - 20 m	20 m	
	20 m - 100 m	30 m	
	> 100 m	40 m	
Thermal Properties			
Volumetric heat capacity	$x \cdot 10^6\ \mathrm{J\,m^{-3}\,K^{-1}}, \quad x \in \{1.5, \mathbf{2}, 2.5\}$	acc. to Noetzli and Gruber (2009)	
Thermal conductivity	$x \cdot \mathrm{W\,K^{-1}\,m^{-1}}, \quad x \in \{2, \mathbf{3}\}$	acc. to Noetzli and Gruber (2009)	
Volumetric fraction	0.05 Water	acc. to Myhra et al. (2017, 2019)	
	0 Ice		
	0 Organic		
	0.95 Rock		
	0 Minimum water		
	1 Sum of fractions		

3 Discussion - Scope of interpretation and limitations to modeling

3.1 Implications and limitations of the mechanical analysis with UDEC

Rock slides in brittle rock are controlled by structural features within the rock mass, which typically are joints, fault zones, and foliation/bedding structures (Hungr et al., 2014). These structures define potential kinematic release surfaces and may concentrate stress. Mechanical simulations with model setups A (explicitly predefined basal shear plane) and B (implicit creation of shear plane through many substructures) yielded similar outcomes. Both setups indicated instability under the same shear parameter combinations and with similar volumes displaced. Simulations reproduced shear failure initiation following the shear activation of the rock slope's toe (topographic knickpoint), highlighting topographic control of the rock slide (compare to Leith et al., 2014). This comparison of model setups suggests that joint spacing and block size play a secondary role compared to the dominant topographic control and the presence of a kinematically feasible or interconnected release surface. While model setup A emphasizes simplicity and abstraction to illustrate the concept of a single main shear plane, model setup B provides a better representation of the progressive failure mechanism - specifically, the evolution of joint slip initiated at the slope's toe and the development of a step-path–shaped failure surface - "en echelon" failure type according to Eberhardt et al. (2004). The brittle rock type, narrow foliation and joint spacing, and less favorable discontinuity orientation - mapped structures do not dip out of the slope (Fig. A1) - likely promoted shear failure along a step-path geometry, involving the shearing of rock bridges to connect discontinuities into an irregular basal shear plane. However, the true basal shear plane could not be reconstructed from surface observations due to the extensive deposits of blocky debris across the slope.

While elastoplastic deformation can be relevant for large-scale slope failures (Rechberger and Zangerl, 2022), it is negligible at the Platteikogel, where the inferred shear plane lies only about 20 m deep. The back-calculated set of shear parameters, which resembles overall pre-failure slope conditions (i.e., $\phi = 30°$ and $c = 0.1$ MPa, Fig. 9a) can be interpreted in regard to field observations. The observed smooth foliation surfaces of the mica schist and gneiss and the highly weathered state of joint surfaces suggest that the natural friction angle ϕ is below 40°. Strauhal et al. (2017), who tested residual friction angle of shear zone material of rock of the same lithologic type, reported residual friction angles between 20 and 30°. The calculated cohesion of 0.1 MPa - as a measure of joint infillings or rock bridges - indicates that for the given pre-failure state, rock bridges were largely degraded. Yet, the actual distribution and percentage of rock brides at pre-failure state, if at all, can only be assessed post-failure (Elmo, 2023) or indirectly via the here presented back-calculation (Kemeny, 2003). The proposed overall shear strength should be interpreted as a combination of discontinuity surface conditions, rock bridges, and heterogeneous ice distribution along cavities or discontinuities.

3.2 Representation and limits of thermal processes in CryoGrid 2D

Permafrost evolves over decades and responds to atmospheric changes with a lag. Its temperature in depths below the active layer is governed mainly by conductive heat transfer (Noetzli and Gruber, 2009; Myhra et al., 2017). Rather than using an energy balance model, we considered only rock surface temperature as long-term model forcing, which was inferred from air temperatures via temperature transfer functions (i.e. see Magnin et al., 2019). Importantly, permafrost evolution is controlled

by long-term air temperature trends (Noetzli et al., 2024). While absolute rock surface temperatures remain highly uncertain due to spatial and temporal heterogenities in snow cover (Haberkorn et al., 2015), or complex 3D terrain with varying aspect, slope, and terrain roughness (Noetzli and Gruber, 2009), a general trend of warming permafrost between 1980 and 2023 was distinctly replicated in our simulation, although true temperatures may slightly vary.

The spatial and temporal scale of the thermal simulation makes field validation unfeasible. Therefore, parameter calibration was conducted for a similar rock type (metamorphic rock) and altitude (Fig. A2a) in order to resemble field conditions. And, to account for uncertainty, we explored ensemble simulations with 100 twins. For details on limitations and constraints of the Cryogrid 2D simulation and strategy, we here refer to the extended discussion in Czekirda et al. (2023), whose modeling concept was adopted and advanced here with the incorporation of ice aprons.

The simulated warming rates are within the European trend measured in bedrock mountain permafrost: Noetzli et al. (2024, Fig. 5d) describe a mean warming of +0.59°C at 10 m below surface for the last 4 decades, while our model suggests decadal warming rates between 0.41 and 0.63°C for the same period and depth in the area of the Platteikogel ridge covering northwestern and southeastern aspects (Table 2).

In our mechanical and conceptual models (Fig. 5), we infer that ice apron loss alters hydrogeological flow paths and promotes hydrostatic pressure buildup. In fractured permafrost rock, percolating water follows predefined pathways (fractures, joints, faults), forming local thaw corridors through advective heat transport (Hasler et al., 2011) — a process not represented in CryoGrid 2D. However, groundwater flow in fractured rock slopes is dependent on the geometry and properties of the fractured rock aquifer, which can only be approximated in slope-scale models through explicitly defined subsurface structures and abstractions made (Magnin and Josnin, 2021). Modeling groundwater in mountainous terrain remains challenging due to complex topography, heterogeneous subsurface properties, and a scarcity of field data forming a research field of its own (Somers and McKenzie, 2020). The omission of advective heat transport is justified by the conductive focus of CryoGrid 2D and the lack of site-specific parameters such as fracture permeability, hydraulic gradients, and transient water fluxes. Our objective was to reproduce long-term permafrost temperature trends, for which conductive modeling provides a robust first-order approximation (Riseborough et al., 2008; Myhra et al., 2017; Czekirda et al., 2023).

References

Buckel, J. and Otto, J.-C.: The Austrian Glacier Inventory GI 4 (2015) in ArcGis (Shapefile) Format, https://doi.org/10.1594/PANGAEA.887415, 2018.

Czekirda, J., Etzelmüller, B., Westermann, S., Isaksen, K., and Magnin, F.: Post-Little Ice Age Rock Wall Permafrost Evolution in Norway, The Cryosphere, 17, 2725–2754, https://doi.org/10.5194/tc-17-2725-2023, 2023.

Eberhardt, E., Stead, D., and Coggan, JS.: Numerical Analysis of Initiation and Progressive Failure in Natural Rock Slopes—the 1991 Randa Rockslide, International Journal of Rock Mechanics and Mining Sciences, 41, 69–87, 2004.

Elmo, D.: The Bologna Interpretation of Rock Bridges, Geosciences, 13, 33, 2023.

Haberkorn, A., Hoelzle, M., Phillips, M., and Kenner, R.: Snow as a Driving Factor of Rock Surface Temperatures in Steep Rough Rock Walls, Cold Regions Science and Technology, 118, 64–75, 2015.

Hasler, A., Gruber, S., Font, M., and Dubois, A.: Advective Heat Transport in Frozen Rock Clefts: Conceptual Model, Laboratory Experiments and Numerical Simulation, Permafrost and Periglacial Processes, 22, 378–389, 2011.

Hungr, O., Leroueil, S., and Picarelli, L.: The Varnes Classification of Landslide Types, an Update, Landslides, 11, 167–194, https://doi.org/10.1007/s10346-013-0436-y, 2014.

Kemeny, J.: The Time-Dependent Reduction of Sliding Cohesion Due to Rock Bridges Along Discontinuities: A Fracture Mechanics Approach, Rock Mechanics and Rock Engineering, 36, 27–38, https://doi.org/10.1007/s00603-002-0032-2, 2003.

Leith, K., Moore, J., Amann, F., and Loew, S.: In Situ Stress Control on Micro-Crack Generation and Macroscopic Extensional Fracture in Exhuming Bedrock, Journal of Geophysical Research, https://doi.org/10.1002/2012JB009801, 2014.

Magnin, F. and Josnin, J.-Y.: Water Flows in Rock Wall Permafrost: A Numerical Approach Coupling Hydrological and Thermal Processes, Journal of Geophysical Research: Earth Surface, 126, e2021JF006 394, https://doi.org/10.1029/2021JF006394, 2021.

Magnin, F., Etzelmüller, B., Westermann, S., Isaksen, K., Hilger, P., and Hermanns, R. L.: Permafrost Distribution in Steep Rock Slopes in Norway: Measurements, Statistical Modelling and Implications for Geomorphological Processes, Earth Surface Dynamics, 7, 1019–1040, https://doi.org/10.5194/esurf-7-1019-2019, 2019.

Myhra, K. S., Westermann, S., and Etzelmüller, B.: Modelled Distribution and Temporal Evolution of Permafrost in Steep Rock Walls Along a Latitudinal Transect in Norway by CryoGrid 2D, Permafrost and Periglacial Processes, 28, 172–182, https://doi.org/10.1002/ppp.1884, 2017.

Myhra, K. S., Westermann, S., and Etzelmüller, B.: Modeling Conductive Heat Flow Between Steep Rock Walls and Talus Slopes – Thermal Processes and Geomorphological Implications, Frontiers in Earth Science, 7, https://doi.org/10.3389/feart.2019.00192, 2019.

Noetzli, J. and Gruber, S.: Transient Thermal Effects in Alpine Permafrost, The Cryosphere, 3, 85–99, 2009.

Noetzli, J., Isaksen, K., Barnett, J., Christiansen, H. H., Delaloye, R., Etzelmüller, B., Farinotti, D., Gallemann, T., Guglielmin, M., Hauck, C., Hilbich, C., Hoelzle, M., Lambiel, C., Magnin, F., Oliva, M., Paro, L., Pogliotti, P., Riedl, C., Schoeneich, P., Valt, M., Vieli, A., and Phillips, M.: Enhanced Warming of European Mountain Permafrost in the Early 21st Century, Nature Communications, 15, 10 508, https://doi.org/10.1038/s41467-024-54831-9, 2024.

Pfluger, F., Weber, S., Steinhauser, J., Zangerl, C., Fey, C., Fürst, J., and Krautblatter, M.: Massive Permafrost Rock Slide under a Warming Polythermal Glacier Deciphered through Mechanical Modeling (Bliggspitze, Austria), Earth Surface Dynamics, 13, 41–70, https://doi.org/10.5194/esurf-13-41-2025, 2025.

Rechberger, C. and Zangerl, C.: Rock Mass Characterisation and Distinct Element Modelling of a Deep-Seated Rock Slide Influenced by Glacier Retreat, Engineering Geology, 300, 106 584, 2022.

Riseborough, D., Shiklomanov, N., Etzelmüller, B., Gruber, S., and Marchenko, S.: Recent advances in permafrost modelling, Permafrost and Periglacial Processes, 19, 137–156, https://doi.org/10.1002/ppp.615, 2008.

Somers, L. D. and McKenzie, J. M.: A Review of Groundwater in High Mountain Environments, WIREs Water, 7, e1475, https://doi.org/10.1002/wat2.1475, 2020.

Strauhal, T., Zangerl, C., Fellin, W., Holzmann, M., Engl, D. A., Brandner, R., Tropper, P., and Tessadri, R.: Structure, Mineralogy and Geomechanical Properties of Shear Zones of Deep-Seated Rockslides in Metamorphic Rocks (Tyrol, Austria), Rock Mechanics and Rock Engineering, 50, 419–438, https://doi.org/10.1007/s00603-016-1113-y, 2017.